International Journal of Fracture **59:** 115–132, 1993.

Effect of geometry on compressive failure of notched composites

M.P.F. SUTCLIFFE and N.A. FLECK
Cambridge University Engineering Department, Trumpington Street, Cambridge CB2 1PZ, UK

Received 10 February 1992; accepted in revised form 10 August 1992

Abstract. The compressive failure of carbon fibre-epoxy laminates is investigated theoretically and experimentally. Panels with a single edge notch, a central notch or a central hole are considered. The failure mechanism is by microbuckling in the 0° plies and is accompanied by delamination and plastic deformation in the off-axis plies [1]. To predict the critical length of the microbuckle and the failure load, the microbuckle is modelled as a cohesive zone. The magnitude of the normal compressive traction across the microbuckle is assumed to decrease linearly with increasing overlap of material on either side of the microbuckle. The relative effect of the specimen size and a bridging length scale is investigated to illustrate the transition between small-scale and large-scale bridging. If the bridging length scale is small compared with the specimen dimensions, the specimen fails when the stress intensity at the notch tip equals a critical compressive stress intensity factor K_{IC}. When the bridging length scale is not small compared with either the initial defect size or the unnotched ligament length then it is necessary to include the details of the traction across the microbuckle to predict the failure load accurately.

1. Introduction

Holes and notches reduce the compressive strength of composite panels. To investigate this reduction in strength three geometries are considered in this paper – centre notched panels, panels with a single edge notch and panels with a central open hole, as illustrated in Fig. 1. Soutis et al. [1] and Guynn et al. [2] find that damage is initiated in multi-directional carbon fibre-epoxy and carbon fibre-PEEK laminates respectively at the edge of holes by fibre microbuckles in the 0° plies. These microbuckles nucleate and grow in a stable manner under an increasing remote load, so that the panel fails at a higher load than that at which damage initiates. Similar behaviour is observed in this paper with blunt notched geometries. We assume that there is a finite slit thickness separating the notch faces, sufficient to prevent contact across the slit faces on loading.

Figure 2 is a simplified schematic diagram of the details of the microbuckling failure in a 0° ply. The microbuckle emanates from the hole or blunt notch tip in a direction approximately transverse to the loading direction [1]. As the microbuckle grows, fibres break behind the microbuckle tip to form a kink band with a width of about 100 μm. Matrix cracking and plasticity in the off-axis plies above and below the microbuckled 0° plies and a zone of delamination between the plies is associated with this microbuckle damage. Both the kink band and these off-axis plies continue to support some load after microbuckling. In Fig. 2 microbuckling is shown in the plane of the specimen and material buckles into the hole or into the notch. In fact more detailed investigation shows that, away from the hole or notch, fibres generally microbuckle out of the plane of Fig. 2 towards the unsupported surfaces [1–3].

In this paper the evolution of damage is studied theoretically using fracture mechanics methods used for bridged cracks. The microbuckled region is treated as a cohesive zone and the intrinsic toughness at the tip of the microbuckle is assumed to equal zero. The two mechanisms of buckling into the hole and buckling out of the plane of the specimen allow the

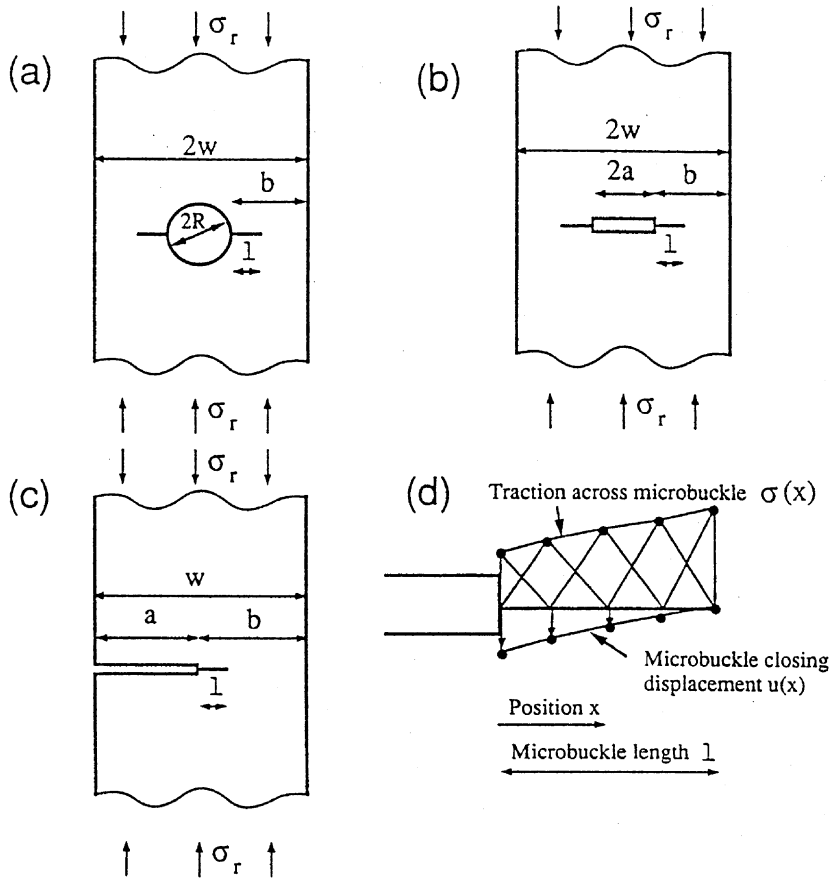

Fig. 1. Geometry of specimens. (a) Central hole, (b) Centre notch, (c) Single edge notch, (d) Details of microbuckle.

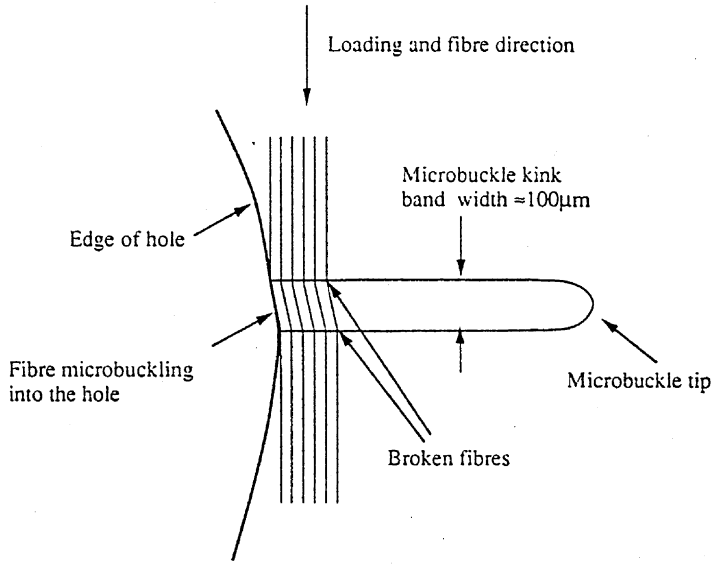

Fig. 2. Schematic diagram of a microbuckle emanating from the edge of a hole in a 0° ply.

material on either side of the microbuckle to approach, as required if the problem is to be modelled as a bridged crack under compressive loading. By contrast with conventional fracture mechanics, where it is assumed that the notch tip is sharp, we have considered here blunt notches. Although initiation of the damage region will be affected by the geometry of the slit tip, as long as the peak load is associated with a damage region significantly longer than the separation of the slit faces, then the details of the slit geometry do not affect that peak load. If the notch and ligament lengths a and b are large compared with the damage zone at failure,

then the behaviour is termed 'small-scale bridging' and the applied stresses at failure are characterised by the compressive stress intensity factor K_{IC}, based on a sharp notch. This critical stress intensity factor is a material property. Measurements of K_{IC} made with a standard blunt notch geometry can then be used to calculate the failure load for other blunt notch geometries and for panels with holes, where similar failure mechanisms apply.

To investigate the situation where, as often occurs in composites, the damage zone at failure is no longer small compared with the specimen dimensions ('large-scale bridging'), we need to look in more detail at the micro-mechanics of the damage region. The way in which the traction across the microbuckle varies with the relative displacement of either side of the microbuckle is an important input into the microbuckle bridging law. Although estimates of this can be made from a microbuckling analysis [4], the values for the resulting toughness of the laminate are too low. Instead the functional form of a bridging law is assumed and its magnitude is established from fracture toughness tests in compression.

Theoretical calculations are presented for all three geometries and experiments are performed for the notched specimens to look at the effects of large-scale bridging. For the specimen geometries shown in Fig. 1 three length scales can be identified: the notch length a or hole radius R, the ligament length b for the undamaged specimen and a bridging length scale r_p. An appropriate bridging scale r_p is given as

$$r_p = \frac{E'G_{IC}}{\sigma_u^2} = \frac{K_{IC}^2}{\sigma_u^2}, \tag{1}$$

where E' is an effective elastic modulus such that $G = K^2/E'$ (defined further in Section 2), G_{IC} is the compressive toughness and σ_u is the unnotched strength of the laminate. Important dependent variables are the remote stress σ_r at failure, the corresponding stress intensity factor K_r based on the notch length, and the critical microbuckle length l_c. For the simple bridging law used in this paper the effect of geometry on the failure behaviour can then be described with a functional relationship of the form

$$\frac{l_c}{r_p}, \frac{K_r}{K_{IC}}, \frac{\sigma_r}{\sigma_u} = f\left(\frac{a}{r_p}, \frac{b}{r_p}\right). \tag{2}$$

By drawing contour or surface plots of the independent variables as a function of a/r_p and b/r_p it is possible to summarise the effects of large-scale bridging on one graph. This provides both a simple qualitative picture of the importance of including a detailed analysis in a particular application and quantitative results for the three geometries with the particular bridging law used here. Although the work has been done to help understand the compressive failure of composites, this analysis is equally applicable to either compressive or tensile failure in other applications where a similar crack bridging analysis is relevant.

2. Calculation method

The microbuckled zone is modelled using linear elastic fracture mechanics, taking results derived for cracks. The calculation method and numerical techniques used in this paper are described by Cox and Marshall [5]. The specimen geometry is given in Fig. 1 with a

microbuckle of length l and a uniform remote compressive stress σ_r. The stress intensity at the tip of the microbuckle is zero. The stress intensity factor K_σ due to a distribution of normal compressive stresses $\sigma(x)$ along the microbuckle at the tip of a microbuckle of length l is given by the integral

$$K_\sigma = \int_0^l \sigma(x) m(l, x)\, \mathrm{d}x, \tag{3}$$

where the weight function $m(l, x)$ can be conveniently found from the point load solution given by Newman [6] for a crack emanating from a central hole and from Tada et al. [7] for a single edge notch and a centre notched panel.

Using the weight function method [8], the crack closing displacement $u_\sigma(x)$ on the microbuckle face (where u is half the relative displacement of the two faces of the microbuckle) for a microbuckle of length l due to normal compressive tractions $\sigma(x)$ on the microbuckle faces is given by

$$u_\sigma(x) = -\frac{1}{E'} \int_0^l m(l', x)\, \mathrm{d}l' \int_0^{l'} \sigma(x') m(l', x')\, \mathrm{d}x'. \tag{4}$$

The weight function method is also used to find the stress intensity factor at the microbuckle tip K_{rm} and the displacements across the microbuckle $u_r(x)$ due to the remote stress for the notched panels, using Bueckner's rule. Briefly, the stress intensity factor is calculated from (3) and the displacements from (4), where now the traction on the crack faces is that along the crack line for a specimen containing no crack. For specimens with a central hole, Newman gives the stress intensity factor at the end of the microbuckle and the displacements due to a remote uniform stress. The net stress intensity factor at the microbuckle tip K_m and the displacements along the microbuckle $u(x)$ are given by the sum of the contributions due to the microbuckle loading and the remote loading

$$K_m = K_\sigma + K_{rm}, \tag{5}$$

$$u(x) = u_\sigma(x) + u_r(x). \tag{6}$$

The compressive traction σ across the microbuckle is related to the closing displacement u across the microbuckle by a functional relationship $\sigma = p(u)$ which is taken in this paper to be a simple linear softening law

$$\begin{aligned} &\sigma/\sigma_u = (1 - u/u_c) \quad \text{for } 0 \leqslant u \leqslant u_c, \\ &\sigma/\sigma_u = 0 \quad \text{for } u > u_c, \end{aligned} \tag{7}$$

where u_c is a critical microbuckle overlap displacement. The appropriate value of u_c is found from the measured toughness G_{IC}, using the assumed variation of microbuckle load with displacement, (7)

$$G_{IC} = \int_0^{u_c} 2\sigma(u)\, \mathrm{d}u = \sigma_u u_c. \tag{8}$$

To solve for the remote stress, (3) and (4) are discretised in a similar way to that described by Cox and Marshall [5]. The microbuckle is divided into a number of elements, as illustrated in Fig. 1(d). The influence functions due to triangular distributions of pressure of height unity centred on the ith node for the stress intensity factor at the microbuckle tip f_i and for the displacement at the jth node g_{ij} are calculated by numerical integration of (3) and (4). Influence functions due to unit remote loading for the tip stress intensity factor f_r and for the displacement at the ith node g_{ri} are found in a similar way. A change of variable was made to account for singularities in the integrations where necessary. The effect of a piecewise-linear stress distribution along the microbuckle on the stress intensity at the microbuckle tip and on the displacements along the microbuckle is found by multiplying the traction $\sigma_i = p(u_i)$ at each of the nodes by the relevant influence coefficient and summing over all the nodes. After including the effect of the remote loading, the relationship between the stresses and the displacements across the microbuckle expressed by (3) and (4) gives a set of $N - 1$ coupled non-linear simultaneous equations, where N is the number of nodes

$$u_i = \sum_{j=1}^{N} p(u_j) g_{ij} + \sigma_r g_{ri} \quad \text{for } i = 1 \text{ to } N - 1. \tag{9}$$

The stress for the Nth node at the microbuckle tip equals the unnotched strength of the material and the displacement there is zero. The additional equation needed to solve for the unknown remote stress is that the stress intensity at the tip of the microbuckle K_m due to the remote stress and microbuckle loading is zero

$$K_m = 0 = \sum_{i=1}^{N} p(u_i) f_i + \sigma_r f_r. \tag{10}$$

Normalised versions of the simultaneous equations are solved by a modified Powell hybrid method using a NAG routine [9]. Increasing the number of nodes from five to ten had a negligible effect on the critical load and results presented are for calculations with ten nodes. Parameter tracking is used to ensure that the starting point for the iteration is reasonable. To find the critical load, the length of the microbuckle is incremented until a maximum load is reached. A more accurate value for the critical microbuckle length is then estimated by cubic interpolation of the load versus microbuckle length curve. With the simple laws considered here there was no subsequent increase in load after the first maximum.

The growth of a damage region with increasing load under conditions of small scale bridging is often represented by 'R-curves'. However Bao and Suo [10] note that this procedure may be misleading with large-scale bridging conditions described here, since the curves then depend on the specimen geometry. In this work, while 'effective' R-curves have been calculated to find the peak load, we will not be concentrating on this sub-critical growth of the damage region, but instead on the conditions at failure.

The calculation method outlined above can be compared to that described by Fett and Münz [11]. Equations (3) and (4) can be combined with the effects of the remote loading to give an integral equation

$$u_\sigma(x) = -\frac{1}{E'} \int_0^l m(l', x)\, \mathrm{d}l' \int_0^{l'} p\{u_\sigma(x') + u_r(\sigma_r)\} m(l', x')\, \mathrm{d}x'. \tag{11}$$

Equation (11) can be solved by the method of successive approximations. In the implementation described by Fett and Munz this integral equation is solved by approximating the displacement function $u_\sigma(x)$ by polynomials and using a least-squares computer routine. This method appears to be useful where the remote stress is known and the stress intensity factor at the tip of the microbuckle is required. Where, as here, we are concerned with finding the maximum load, while specifying the tip stress intensity factor, it is simpler to include (10) for the tip stress intensity factor as one of the equations in the solving routine and solve for the applied load.

The weight functions used here are for isotropic materials but the composites considered are orthotropic. Suo et al. [12] show that results for orthotropic materials are dependent on two parameters, $\lambda = E_2/E_1$ and $\rho = (E_1 E_2)^{1/2}/2\mu_{12} - (\nu_{21}\nu_{12})^{1/2}$, where E is the Young's modulus, μ is the shear modulus and ν is Poisson's ratio for the laminate. Subscripts 1 and 2 refer to directions perpendicular and parallel to the remote stress respectively. The equivalent elastic modulus for orthotropic materials E' is given by Sih et al. [13]; in terms of the above elastic constants $E' = \lambda^{1/4}\{(2E_1E_2)/(1+\rho)\}^{1/2}$. For $\rho = 1$, results for isotropic materials can be applied to orthotropic materials by rescaling the dimensions of the problem. Where, as for the notched specimens, there is no significant length scale in the direction normal to the crack, the stress intensity results for orthotropic materials with $\rho = 1$ are the same as for isotropic materials. Although there will be a dependence on ρ for $\rho \neq 1$, Sweeney [14] and Kaya and Erdogan [15] show that this is small for notched specimens. For the specimens with microbuckles emanating from holes there is no suitable set of weight functions for orthotropic materials. Where the microbuckle is small compared with the hole and specimen dimensions, Suo et al. [12] give the asymptotic solution for the stress intensity factor K_{rm} at the microbuckle tip with remote loading σ_r

$$K_{rm} = Y\sigma_r\sqrt{\pi l} = \sigma_r\sqrt{\pi l}(1 + \sqrt{2(1+\rho)})\lambda^{1/4}\{1.12 - 0.011(\rho - 1)\}. \tag{12}$$

Equation (12) is derived by combining the stress concentration factor due to a hole with the single edge notch solution given by Sweeney [14]. For the laminates considered in this paper the above formula yields values of Y in the range 2.8 to 3.9, compared with 3.36 for isotropic theory, indicating that the errors in using isotropic stress intensity solutions for these orthotropic materials are not too large. As the microbuckle becomes significantly longer than the hole diameter the effect of the hole becomes small and the solution tends to the notched results, where the effect of orthotropy is negligible. In this paper the weight functions derived for isotropic materials will be used to approximate the orthotropic results.

3. Results of bridging analysis

The nature of the crack bridging solution is dependent upon the non-dimensional geometrical variables a/r_p and b/r_p. For the centre notched geometry details of the behaviour at the critical load are given. While these details will depend on the details of the bridging law, the general behaviour observed will be similar for similar bridging laws [10]. Since the behaviour for the single edge notch specimen and for the panel with a central hole is similar to that for the centre notch specimen, only a summary of the results will be given for those cases.

3.1. Centre notched panel

Results are given in Figs. 3 to 6 for the centre notched panel. Figure 3 plots contours of the critical microbuckle length l_c at failure, normalised by r_p. Figure 4 is a surface plot of the ratio of the stress intensity factor K_r based on the notch length and the remote stress at failure to the critical stress intensity factor K_{IC}. Figure 5 shows the average stress across the ligament σ_n $(=\sigma_r w/b)$ normalised by the unnotched strength σ_u and Fig. 6 gives the stress distribution across the microbuckle at failure for some typical cases. For $b \gg r_p$ results agree with those calculated by Bao and Suo for an infinite plate [10]. There are three distinct regimes of behaviour as

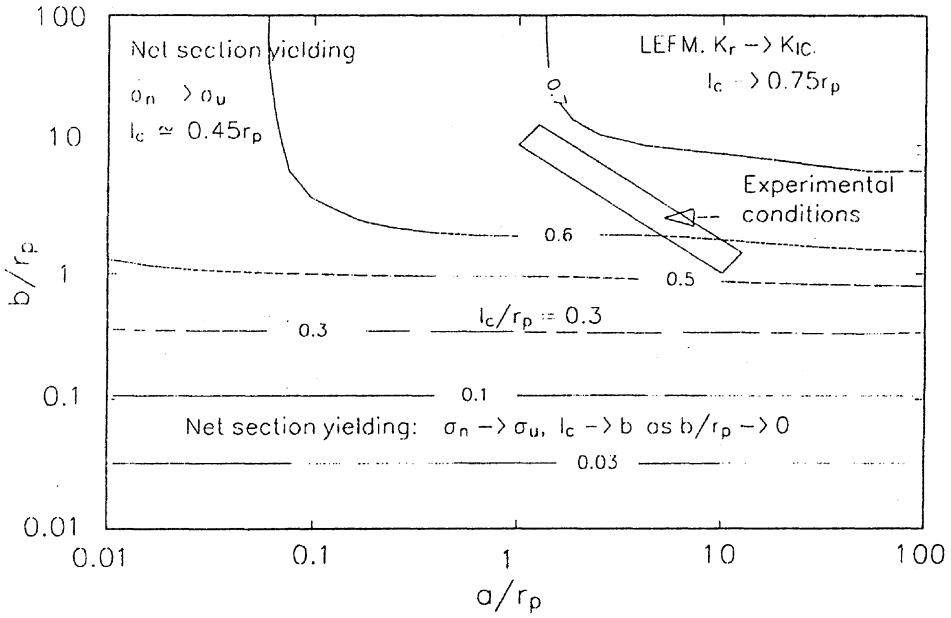

Fig. 3. Regimes of behaviour and contours of the ratio of the critical microbuckle length l_c to the bridging length scale r_p for centre notched specimens.

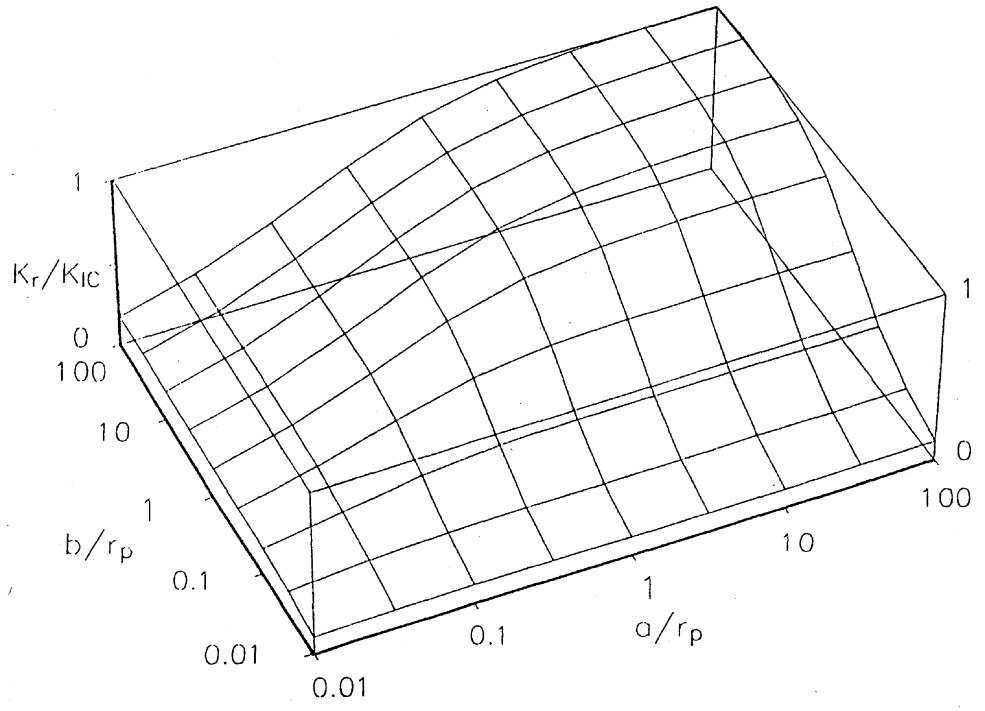

Fig. 4. Theoretical stress intensity factor ratio K_r/K_{IC} at failure, based on notch length, for centre notched specimens.

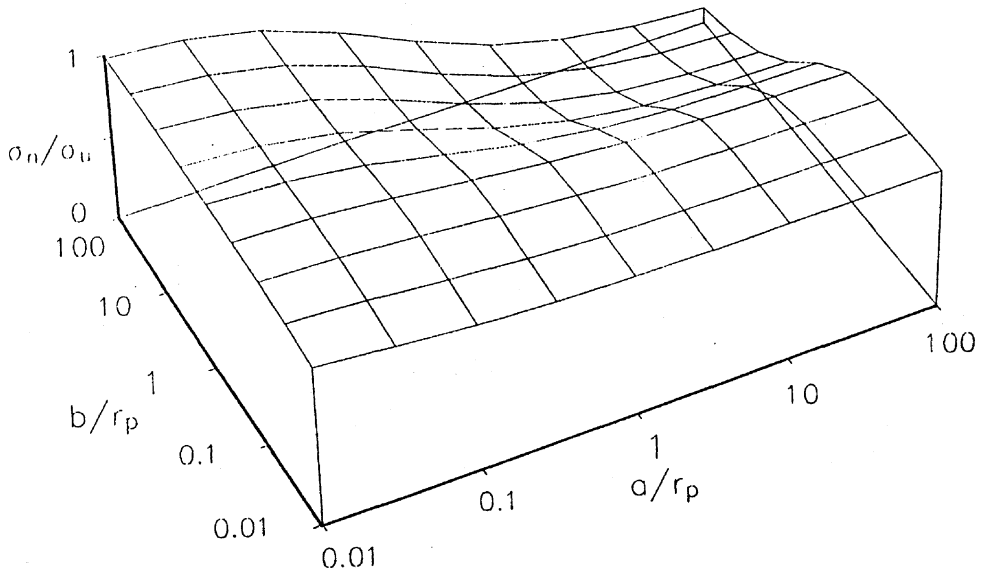

Fig. 5. Theoretical ratio σ_n/σ_u $(=\sigma_r w/\sigma_u b)$ of the net section stress across the ligament to the unnotched strength for centre notched specimens.

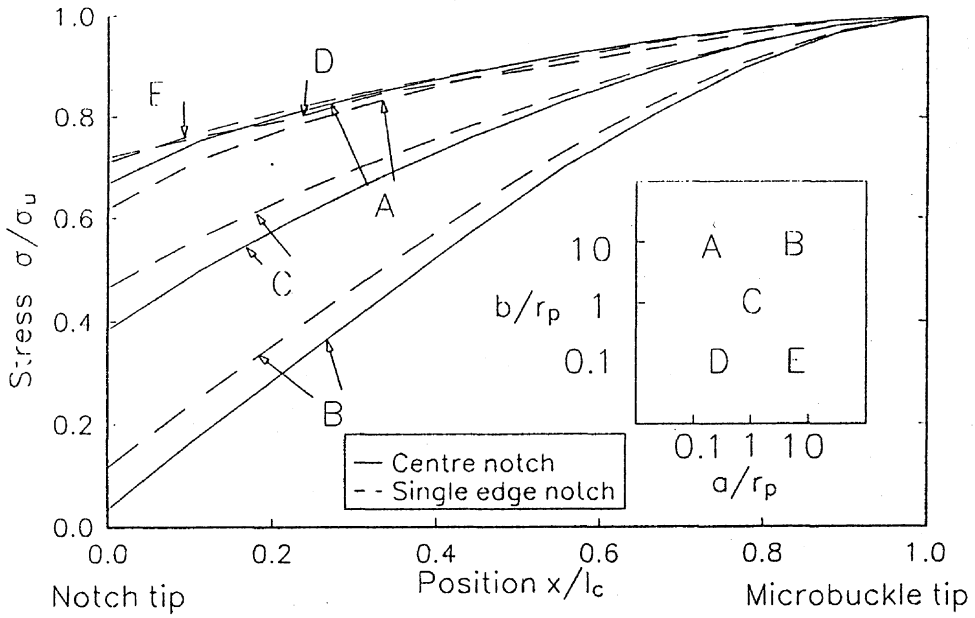

Fig. 6. Theoretical pressure distribution across the microbuckle at failure for centre notched and single edge notched specimens. Inset gives a key to labelling.

summarised in Fig. 3. We deal with each regime in turn and give asymptotic solutions (described in the Appendix) for the critical microbuckle length and the failure load.

3.1.1. Regime I: small scale bridging

Small scale bridging conditions exist when the bridging length scale r_p is much less than the ligament length b and the notch length a. Figure 4 shows that the stress intensity factor K_r (based on the notch length and the remote stress) equals the critical stress intensity factor K_{IC}. In this regime the details of the damage zone do not affect the failure load. At failure the traction across the microbuckle at the notch tip drops almost to zero, as shown in curve B of Fig. 6. The limiting case appropriate for this regime, with a microbuckle emanating from a semi-infinite notch in an infinite body, shows that the microbuckle length at failure tends to $0.75r_p$ as a/r_p and b/r_p tend to infinity, confirming the role of r_p in determining the bridging length scale. This can

be compared with a Dugdale analysis for the same geometry, in which the bridging tractions are equal to the unnotched strength σ_u, for u less than u_c and equal to zero for $u > u_c$. This gives a critical microbuckle length of $0.39r_p$; thus the length of the damage region at failure depends on the particular choice of bridging law.

3.1.2 Regime II: $a \ll r_p$, $b \gg r_p$

When the notch length a is small compared with the bridging length scale but the ligament length b is large compared with r_p, the effect of the notch on the critical load is unimportant and the net stress in the ligament equals the unnotched strength, as shown in Fig. 5. The traction at the notch tip is no longer zero, but in the case chosen with $a/r_p = 10$, $b/r_p = 0.1$ the traction at the notch tip equals about $0.7\sigma_u$ (curve A in Fig. 6). The asymptotic analysis appropriate for this regime with a finite crack in an infinite body shows that, as a/r_p tends to zero, the critical microbuckle length tends to about $0.45r_p$ (Fig. 3). This value of critical microbuckle length depends on the assumed bridging law; for a Dugdale-type law with finite u_c the critical microbuckle length is much greater than r_p.

3.1.3. Regime III: $b \ll r_p$

Now consider the case where the ligament length b is small compared with r_p. For b/r_p less than about 0.3 calculations show that the load continues to increase with increasing microbuckle length for l/b up to 0.95. Beyond this the weight functions used become unreliable. When a maximum is not reached before this point, the maximum microbuckle length is plotted on Fig. 3 as b and the remote stress at failure is taken as the value for $l/b = 0.95$. In this regime the microbuckle displacements along the entire microbuckle length are small compared with the characteristic displacement u_c until just before failure and the microbuckle stress is close to the unnotched strength.

The full asymptotic calculation for this geometry has not been performed, but results will be similar to those for the single edge notched geometry given in the Appendix. A simplified analysis for a/r_p large, using the results of Benthem and Koiter [16], shows that the net section stress across the original uncracked ligament at failure tends to the unnotched strength, as b/r_p tends to zero. For finite b/r_p the maximum load is reached before the microbuckle extends completely through the ligament and is only slightly above the value of remote load at $l/b = 0.95$, as assumed earlier.

3.2. Single edge notched specimen

Contours of the ratio of the critical microbuckle length l_c to the bridging length scale r_p for the single edge notched specimen are shown in Fig. 7. The effect of geometry on the failure load is illustrated in Fig. 8 by showing a surface plot of the variation of the parameter $\sigma_n w/(\sigma_u b)$ with the length ratios a/r_p and b/r_p. This normalisation of the applied stresses is suggested by the asymptotic solution for small b/r_p, as described in the Appendix. Theoretical stress distributions across the microbuckle at failure are included on Fig. 6. In order to compute accurately the solution for the finite geometry (Figs. 6–8) as the intact part of the ligament becomes small compared with the other specimen dimensions, it was found necessary to use the weight function solution given by Tada et al. [7] for a crack approaching a free edge in a semi-infinite plate. For the cases where this modification was made (i.e. where the intact part of the ligament was less than one-tenth of the specimen width) this approach gives a good approximation to the weight function for the single edge notched geometry.

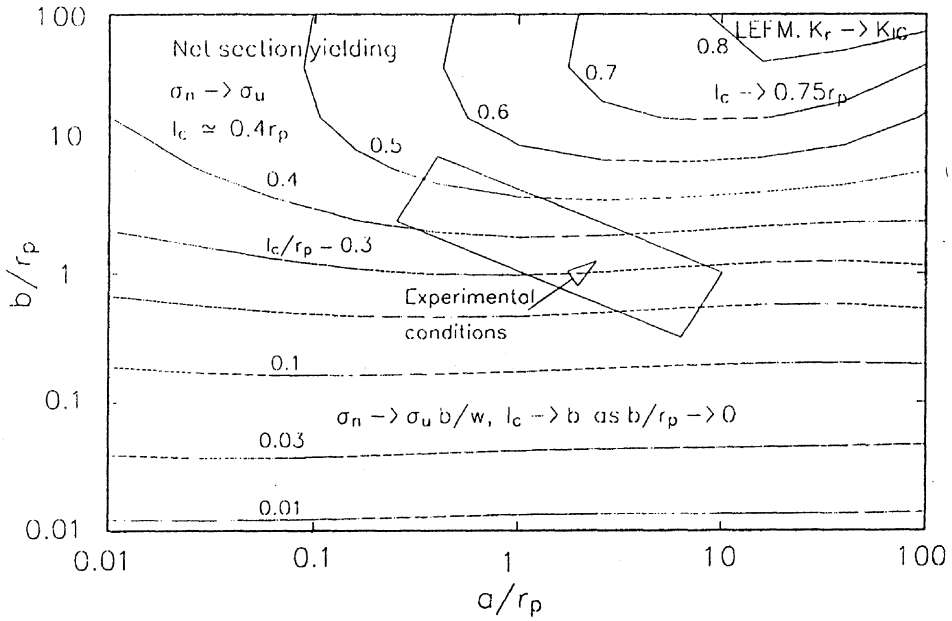

Fig. 7. Regimes of behaviour and contours of the ratio of the critical microbuckle length l_c to the bridging length scale r_p for single edge notched specimens.

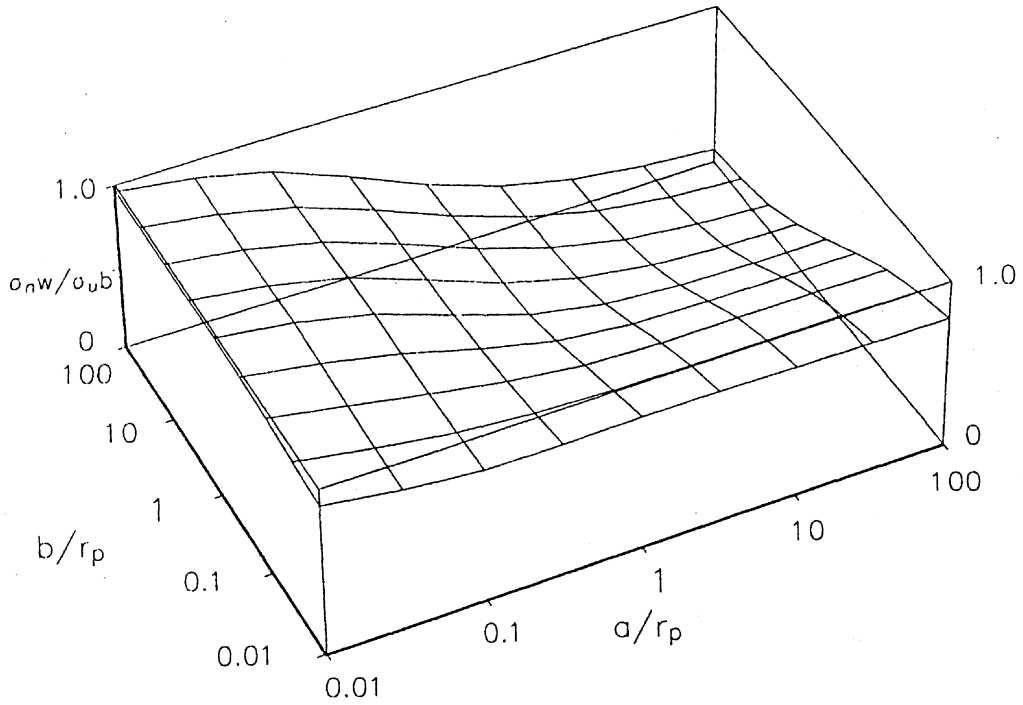

Fig. 8. Theoretical ratio $\sigma_n w/\sigma_u b$ $(=\sigma_r w^2/\sigma_u b^2)$ showing the effect of geometry on applied stress for single edge notched specimens.

Results for the single edge notched specimens are very similar to those for the centre notched specimens. The only important difference is that, for small b/r_p, the net section across the ligament tends to $\sigma_u b/w$ at failure, compared with the value of σ_u for the centre notched panels. Consider the case of the single edge notched specimen with b/r_p and b/a small. An asymptotic solution is given in the Appendix for this case. Maximum load occurs when the microbuckle is near to the free edge of the specimen, at $l \sim b$. The stress intensity factor K_σ due to the microbuckle loading scales as $\sigma_u b^2$. The stress intensity K_{rm} due to the remote loading scales as $\sigma_r w^2$ and balances K_σ for the total stress intensity to vanish at the tip of the microbuckle. Thus σ_r tends to $\sigma_u b^2/w^2$ as b tends to 0 and the net section stress tends to $\sigma_u b/w$.

In this paper tensile failure in the intact ligament has not been considered. However, for the edge notched specimen with b/r_p small, the tensile stress across the intact ligament is significantly larger than the unnotched compressive strength σ_u when the microbuckle length is much larger than the intact ligament length. Where the tensile strength is of the order of the compressive strength the theory should then be modified accordingly to allow for this failure mechanism.

3.3. *Panel with a central hole*

For a panel with a central hole, it is not possible to cover such a wide range of cases as for the notched specimens, since the formulae given by Newman are only valid for $R/w < 0.25$ and $(R + l)/w < 0.75$. Figure 9 is a contour plot of the critical microbuckle length at failure. Figure 10 shows the net failure stress across the ligament for the range of values that can be considered. The results agree with the calculations of Soutis et al. [1] using the stress intensity results of Newman in a slightly different way. These results are similar to those for the notched specimens except in the region where R/r_p is greater than 1. For $R/r_p > 10$ the specimens with a central hole fail when the local stress at the hole due to the stress concentration equals the unnotched strength, with no stable microbuckle growth. Bao and Suo [10] find that the corresponding transition to unstable growth occurs for $R/r_p > 20$ with a Dugdale bridging law. For the analogous case of a notched specimen with large a/r_p failure occurs at $K_r = K_{IC}$.

4. Experimental work

Experimental measurements of the compressive failure load for two lay-ups of T800/924C carbon fibre-epoxy laminates have been made for the centre notched and single edge notched configurations using the test set-up described in [1]. The lay-ups used were $[\pm 45°/0°_2)_3]_s$ and $[(\pm 45°)_2/0°/(\pm 45°)_2/0°/\pm 45°]_s$, denoted as lay-ups L2 and L6 respectively, following Soutis et

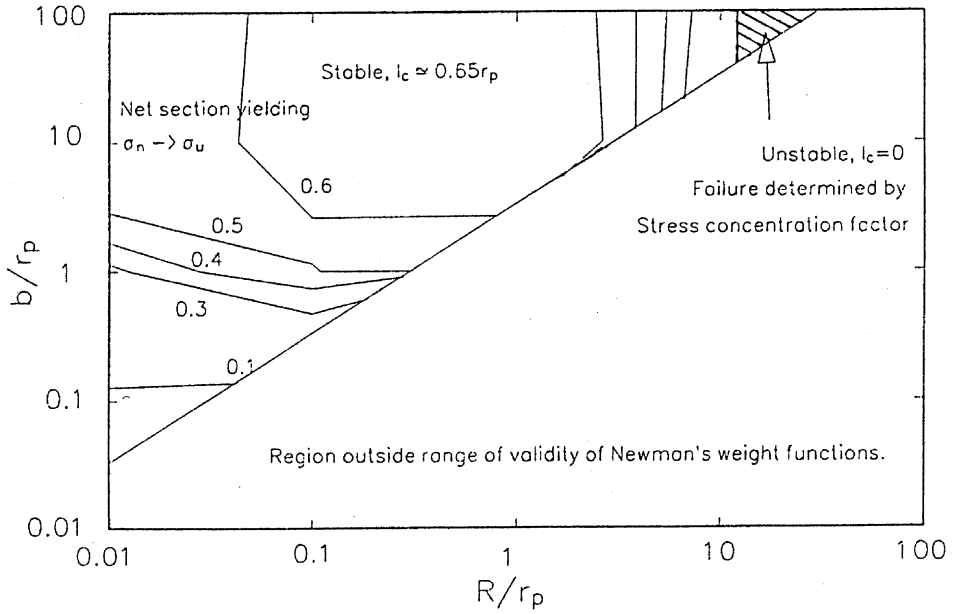

Fig. 9. Regimes of behaviour and contours of the ratio of the critical microbuckle length l_c to the bridging length scale r_p for specimens with a central hole.

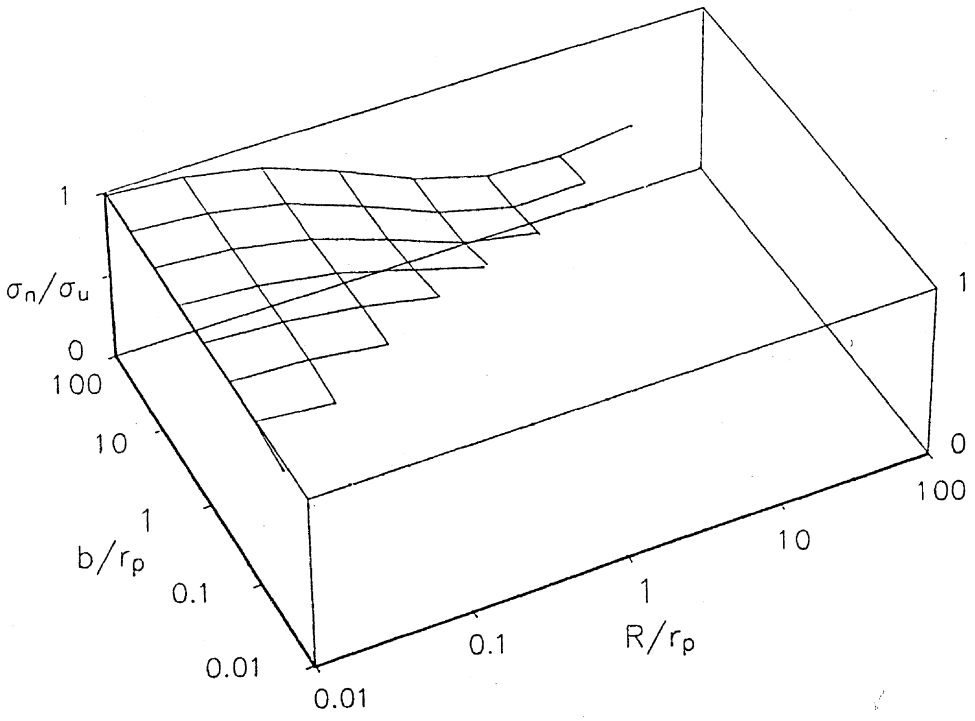

Fig. 10. Theoretical ratio σ_n/σ_u $(=\sigma_r w/\sigma_u b)$ of the net section stress across the ligament to the unnotched strength for specimens with a central hole.

al. [17]. These lay-ups were chosen to give a wide range in compressive properties. The unnotched strengths σ_u of the laminates were 810 and 428 MPa for the L2 and L6 lay-ups. The corresponding orthotropic elastic constants were $\lambda = 3.6$ and 1.6, and $\rho = 0.67$ and -0.09 respectively. The thickness of each panel was 3 mm and specimen widths of 30 and 50 mm were used. The gauge length of the specimens was 115 mm. An anti-buckling guide was used to prevent macro-buckling and the specimens were loaded through wedge grips (see [17] for further details). The jewellers saw made to cut the slits had a 0.7 mm thick blade. The notch tip was sharpened with a razor blade. This arrangement ensured that the slit faces did not close up on loading until after the maximum load had been reached. In all the cases investigated stable growth of the microbuckle was observed and the damage zone length at failure was significantly larger than the slit separation, justifying the use of the stress intensity factor based on a sharp notch to characterise the applied load. The failure load was found to be the same for sharpened specimen as for specimens with notch tips which were not sharpened with a razor blade, confirming that the details of the notch geometry are unimportant at failure.

In the design of the tests two aspects of interest have been addressed. Firstly the analysis shows that, when the bridging length scale r_p is small compared with the specimen dimensions, the critical load corresponds to $K_r = K_{IC}$. The length scale of the bridging zone r_p is calculated from the measured values of K_{IC} and σ_u using (1). When the bridging length scale is no longer small, a more sophisticated analysis is necessary to estimate the failure load. Experiments can be used to check the generality of K_{IC} as a failure criterion for conditions of small scale bridging for different geometries and to estimate the bridging length scale given by (1). Secondly, it is important to investigate how well the bridging calculation can predict failure loads with large-scale bridging. Soutis et al. [1] show that it is possible to predict accurately the compressive strength of panels with central holes from fracture toughness measurements using a centre notched specimen. Here, we consider the single edge notched specimen and examine the effect of specimen width.

4.1. Results for centre notched panels

Experimental data for the remote stress intensity factor at failure (based on the notch length) taken from Soutis et al. [17] and from the current study are presented in Fig. 11 for the centre notched specimens. The approximate range of conditions covered is included in Fig. 3. Soutis et al. assumed that $r_p/a \ll 1$ and $r_p/b \ll 1$ and thus $K_r = K_{IC}$ at failure. In this paper the value of K_{IC} is estimated by fitting theoretical calculations of K_r (including the effect of bridging) at failure to the combined experimental measurements of [17] and those of the current study. The fit is made for the 50 mm wide specimens over the central portion of the curves in Fig. 11, where the effect of the bridging model on K_r and hence on the estimate of K_{IC} is least. The fitted values of K_{IC} are 52.5 MPa$\sqrt{m}$ and 51.1 MPa$\sqrt{m}$ respectively for the L2 and L6 lay-ups, giving values for r_p of 4.2 mm and 13.3 mm, respectively. These values are somewhat larger than those estimated by [17] because of the allowance made here for microbuckle bridging in estimating K_{IC}. As shown in Fig. 11, the theory predicts a significant effect of bridging on the failure stress for the specimen sizes used, with K_r less than K_{IC}. For the lay-up L6 the predicted values of microbuckle length at failure (approximately equal to $0.6r_p$) are significantly larger than those measured by [17]. This is not surprising since lay-up L6 is composed primarily of 45° plies: the simple microbuckle model used here may be inadequate for this laminate and a more detailed consideration of off-axis deformation and delamination must be included to model the failure.

Figure 11 shows that the theory is in reasonable agreement with observed strengths for the centre notched panels. Experiments confirm that the stress intensity at failure changes only slowly in the region where the bridging length r_p is small compared with other specimen dimensions so that conditions are close to that of small-scale bridging. At the extremes of small and large notches the stress intensity drops significantly below this peak value as large-scale bridging effects become important. The data for the two widths of lay-up L2 support the prediction of a slight dependence of K_r on width.

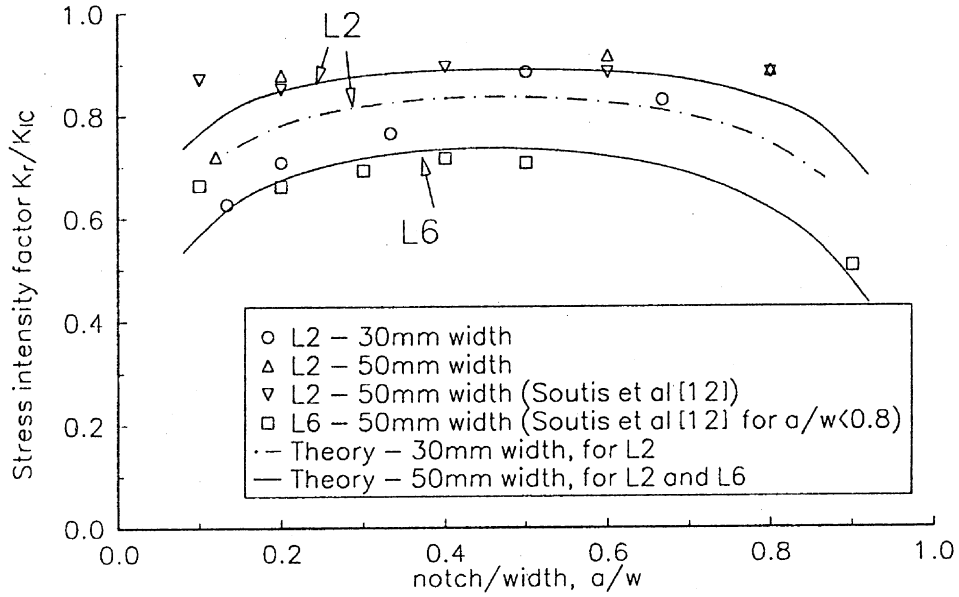

Fig. 11. Measured ratio of the stress intensity factor K_r at failure (based on notch length) to the critical stress intensity factor K_{IC}, for centre notched specimens. K_{IC} is deduced by fitting the theory for 50 mm wide specimens giving K_{IC} = 52.5 and 51.5 MPa$\sqrt{m}$ for L2 and L6 respectively.

4.2. Single edge notched specimens

For experiments with single edge notched specimens two methods of end support were used. In the first set of tests the ends of the specimen were loaded through metal tabs using a wedge clamp arrangement (as for the centre notched specimens). However it was clear, particularly for the specimens with only a small ligament, that this loading arrangement did not produce a uniform remote stress. The clamps allowed little rotation of the ends of the specimen so that a moment was applied by the end grips to counter the tendency for these unsymmetrical specimens to rotate. To investigate this effect, several specimens were loaded through pins placed along the centre line of the specimens. The distance from the pin to the notch line was two to three times the total width of the specimen. End rotation of the specimen is made possible by the pins, and the loading condition is approximately uniform remote loading.

Experimental results for single edge notched specimens are presented in Figs. 12 and 13, and the corresponding range of experimental conditions is shown in Fig. 7. The experimental values of K_r shown in Fig. 12 are calculated using the single edge notch formula for open cracks given by Tada et al. [7], and are normalised by the value of K_{IC} deduced from the centre notched specimens including the effects of bridging. Figure 12 shows that the loading arrangement for single edge notched specimens has a considerable effect on the failure load, particularly for the longer notch lengths; the clamped specimens are up to eight times stronger than the pin loaded specimens. For the pin loaded specimens, measured values of K_r based on the single edge notch calibration are in broad agreement with the theoretical curve for uniform end loading, which has been calculated including microbuckle bridging using the value of K_{IC} deduced from the centre notched specimens. The theory predicts a slight drop in K_r at small and large notch lengths. However the experiments are not able to confirm this feature, since the magnitude of the drop is small compared with the experimental scatter.

For a specimen loaded through clamps, the effect of imposing no end rotation is to make the specimen behave in a similar manner to half of a centre notched specimen with uniform remote loading, particularly as the ligament becomes small compared with the notch length. The remote

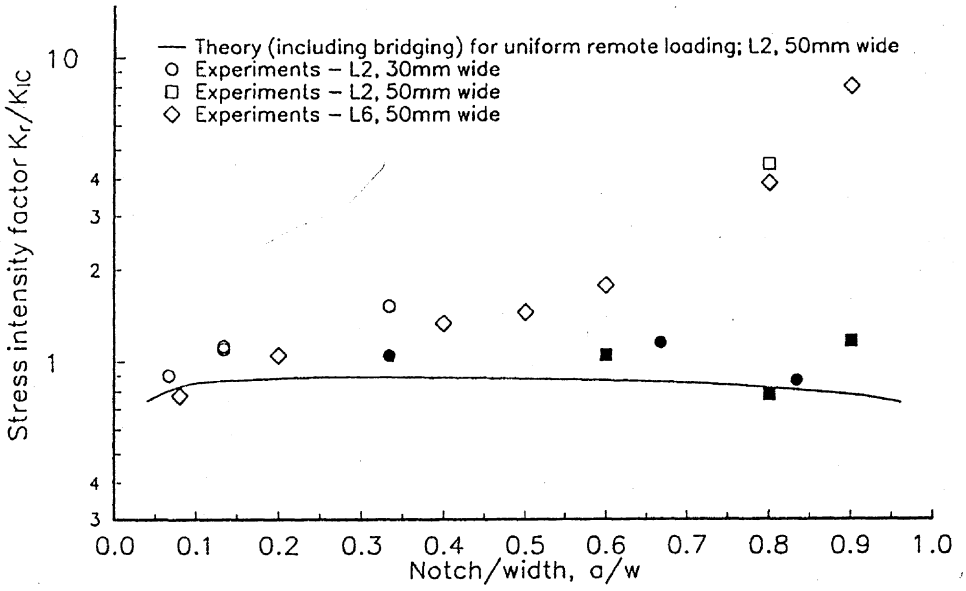

Fig. 12. Measured ratio of the stress intensity factor K_r at failure (based on notch length and uniform remote loading for a single edge notched specimen) to the critical stress intensity factor K_{IC}, for single edge notched specimens. Filled symbols are for pin loading, open symbols for clamp loading.

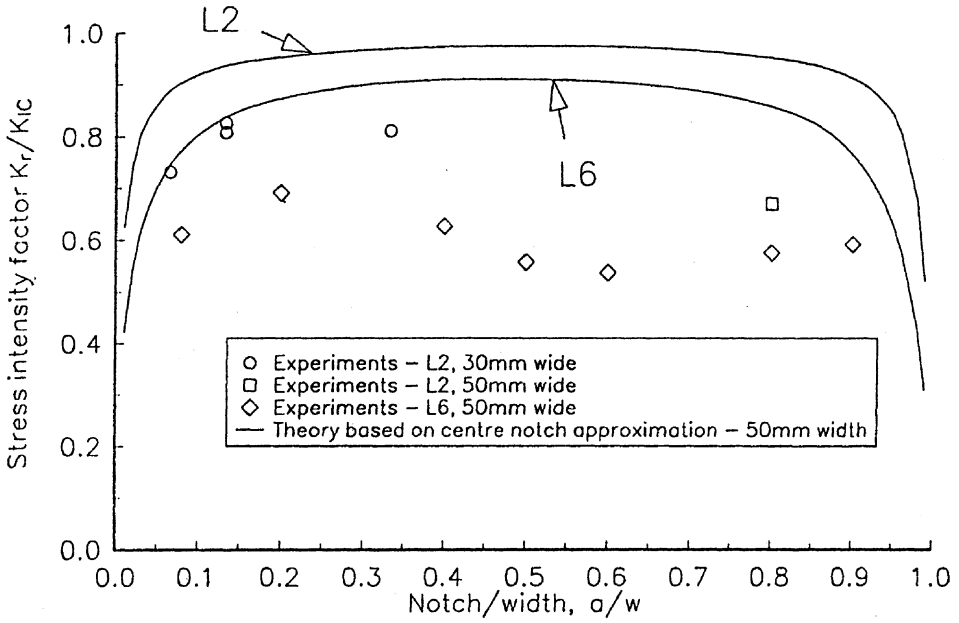

Fig. 13. Measured ratio of the stress intensity factor K_r at failure (based on the centre notch approximation) to the critical stress intensity factor K_{IC}, for single edge notched specimens with clamp loading.

stress intensity factor K_r can then be estimated by treating the specimen as one half of a centre notched specimen, and by using the appropriate K calibration given by [7]. Figure 13 plots this value of K_r for the clamped specimens, normalised by the value of K_{IC} deduced from the specimens with a centre notch. The theoretical values for the remote stress intensity factor at failure included in this figure are found from a bridging analysis using the value of K_{IC} measured from the centre notched panels, again treating the specimen as half of a centre notched specimen. The assumption that the clamped panel behaves like half of a centre notched panel appears to be a good one, with the values of K_r at failure calculated in this way now much closer to the theoretical value. The slight overestimate of the failure load given by this approximation is consistent with a small amount of rotational freedom of the grips.

5. Conclusions

Theoretical calculations and experiments have been performed to investigate the effect of large-scale bridging on compressive failure of carbon fibre epoxy laminates with a hole, a centre notch or a single edge notch. Stable damage growth under increasing load due to microbuckling in the 0° plies is modelled using a crack bridging analysis. The intrinsic tip toughness is assumed to be zero and a linear softening law is used to describe the relationship between the displacements and the bridging tractions across the microbuckle. Results are presented for conditions at the peak load. While the work is motivated by the need to model the compressive failure of composites, it will have relevance to either compressive or tensile failure in other materials where such a bridging analysis is relevant. There are three length scales in the problem: the bridging length scale r_p, the notch length a or radius R, and the ligament length b. The bridging length scale r_p, given by (1), is a material parameter which depends for composites on the laminate lay-up.

Figures 3 and 7 summarise the effect of geometry on the failure mechanisms for different values of the ratios a/r_p and b/r_p for the centre notched and single edge notched specimens.

Asymptotic results are given for the net stress across the ligament and the stress intensity at failure in three regimes. The transition between these extremes is given in Figs. 4, 5 and 8. The behaviour is very similar for these two geometries. Where the bridging length scale is small compared with the specimen dimensions (small-scale bridging), the stress intensity at failure is given by the critical stress intensity factor K_{IC}. The critical microbuckle length is 0.75 times the bridging length scale r_p. As the bridging length becomes comparable with the specimen dimensions an analysis ignoring the local effect of the bridging zone is no longer adequate. The figures quantify this transition for the linear softening law used and give results which will be qualitatively similar for similar bridging laws. For large b/r_p but small a/r_p, the specimen fails when the net section stress equals the unnotched strength and the critical microbuckle length is approximately equal to $0.45r_p$. As b/r_p tends to zero, the critical microbuckle length tends to the ligament length for both notch geometries. For the centre notched panel the net section stress across the ligament tends to the unnotched strength σ_u while for the single edge notch the net section stress tends to $\sigma_u b/w$.

Experimental results for the centre notched panel are used to deduce values of the critical stress intensity factor K_{IC} and hence the bridging length scales for two laminate lay-ups. For intermediate ratios of the notch length to the specimen width, where the critical microbuckle length is relatively small compared with the specimen dimensions, the applied stress intensity factor at failure is roughly constant as expected for small-scale bridging. When the bridging length scale is not small compared with either the notch or ligament lengths, experiments confirm the theoretical predictions of a smaller stress intensity at failure, although results are not so accurate as to confirm the accuracy of the particular bridging law used. Here, evaluation of the stress intensity factor is based on the initial notch length.

The failure load for single edge notched panels is observed to be sensitive to the specimen loading arrangement. If the load is applied via the wedge grips, the lack of rotational freedom at the ends of the specimen makes the specimen behave more like half of a centre notched specimen with a significantly higher failure load than the equivalent pin-loaded specimen. When the effect of the loading arrangement is included, experimental results agree with theoretical predictions, with failure given when the applied stress intensity factor equals the critical stress intensity factor measured from the centre notched geometry.

Theoretical calculations for falure from a central hole are presented in Figs. 9 and 10. These results agree with those of Soutis et al. Where the bridging length is of the order of the hole radius the critical microbuckle length is approximately $0.7r_p$. For r_p much smaller than the hole radius, a maximum load occurs when the local stress at the edge of the stress raiser equals the unnotched strength.

Appendix

Asymptotic solutions for a number of specimen geometries are described in this Appendix. The asymptotic behaviour for the centre notched specimen with $a \ll r_p \ll b$ is investigated by considering the case of a finite notch in an infinite body under uniform remote normal loading. The calculation method described above for finite specimens is used in this analysis with slight modifications. The weight functions for point loads applied at the microbuckle faces, the effect of the remote loading on the microbuckle displacements and the stress intensity factor at the microbuckle tip due to remote loading are all taken from [7]. As a/r_p tends to infinity, the

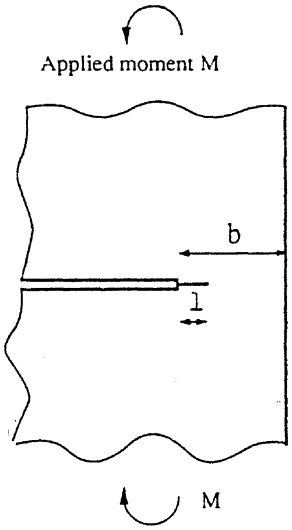

Fig. A1. Geometry of semi-infinite body with a semi-infinite notch.

critical microbuckle length tends to about $0.45r_p$ and the maximum remote stress tends to the unnotched strength σ_u.

The limiting behaviour for small scale bridging with a/r_p and b/r_p tending to infinity is investigated in a similar way by analysing the case of a microbuckle emanating from a semi-infinite notch in an infinite body, using the calculation method described above. For this case the maximum stress intensity factor K_r due to the remote loading equals K_{IC} and the critical microbuckle length l_c is $0.75r_p$.

The geometry shown in Fig. A1 is used to investigate the asymptotic behaviour as a microbuckle extends through the ligament and approaches the free surface in a semi-infinite notched body. A bending moment M is applied. With this loading arrangement the body resembles a single edge notched specimen with a/b and a/r_p large, under uniform remote normal loading. Appropriate dimensionless forms of the dependent variables of interest, the applied moment $2M/\sigma_u b^2$ and the microbuckle length l_c/b at failure, depend only on the ratio of the ligament length b to the microbuckle bridging length scale r_p.

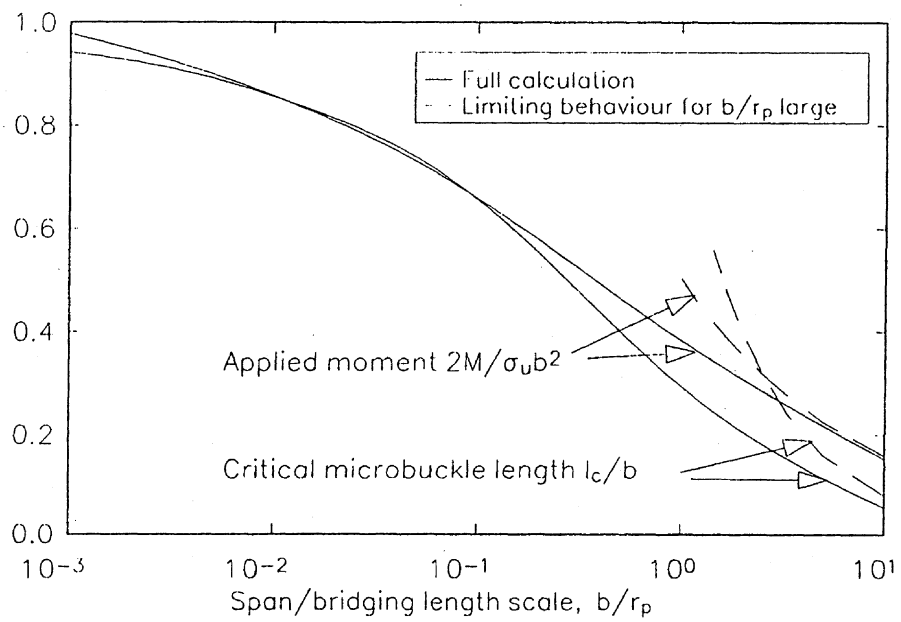

Fig. A2. Asymptotic behaviour for a semi-infinite body with a semi-infinite notch under applied bending.

Results from this calculation are given in Fig. A2. As b/r_p tends to zero the dimensionless applied moment tends to 1 and the maximum load is attained as the microbuckle reaches the free surface. As b/r_p tends to infinity the maximum applied moment and the critical microbuckle length tend to the limit found above for small scale bridging, with the stress intensity factor due to remote loading equal to K_{IC} and the microbuckle length equal to $0.75r_p$.

Acknowledgements

This work was carried out with financial support to one of the authors (MPFS) from the Procurement Executive of the Ministry of Defence and the Science and Engineering Research Council. Support from the ONR contract 00014-91-J-1916 is gratefully acknowledged. The authors wish to thank Dr. P.T. Curtis for helpful discussions, and Mr. R. Brand and Mr. J. Coleman for help with manufacturing the specimens.

References

1. C. Soutis and N.A. Fleck, *Journal of Composite Materials* 24(5) (1990) 536–558.
2. G.E. Guynn and W.L. Bradley, *Journal of Composite Materials* 23 (1989) 479–504.
3. M.P.F. Sutcliffe and N.A. Fleck, in *Proceedings of the ECCM Composites Testing and Standards*, Amsterdam (1992).
4. B. Budiansky and N.A. Fleck, *Journal of the Mechanics and Physics of Solids* (1991) submitted.
5. B.N. Cox and D.B. Marshall, *Acta Metallurgica et Materialia* 39 (1991) 579–589.
6. J.C. Newman, in *Proceedings of the AGARD Conference on the Behaviour of Short Cracks in Airframe Components*, France (1982).
7. H. Tada, P.C. Paris and G.R. Irwin, *The Stress Analysis of Cracks Handbook*, 2nd edition, Paris Productions Inc. (1985).
8. P.C. Paris, R.M. McMeeking and H. Tada, in *Cracks and Fracture, ASTM STP 601* (1976) 471–489.
9. *The NAG Fortran Library Manual – Mark II*, Numerical Algorithms Group, Oxford (1986).
10. G. Bao and Z. Suo, *Applied Mechanics Reviews* (1992) to be published.
11. T. Fett and D. Munz, Kernforschungszentrum Karlsruhe, Rept. No. KfK 4940 (1991).
12. Z. Suo, G. Bao, B. Fan and T.C. Wang, *International Journal of Solids and Structures* 28 (1991) 35–248.
13. G.C. Sih, P.C. Paris and G.R. Irwin, *International Journal of Fracture Mechanics* 1 (1965) 189–203.
14. J. Sweeney, *International Journal of Fracture* 37 (1988) 233–241.
15. A.C. Kaya and F. Erdogan, *International Journal of Fracture* 16 (1980) 171–190.
16. J.P. Benthem and W.T. Koiter, in *Methods of Analysis of Crack Problems*, G.C. Sih (ed.), Noordhoff International (1972).
17. C. Soutis and N.A. Fleck, *Proceedings of the Royal Society, London* (1991) submitted.